Progress In Electromagnetics Research, PIER 15, 109–139, 1997

ANALYTICAL MODELS FOR DETERMINATION OF COMPLEX PERMITTIVITY

J. A. K. Adopley, D. G. Dudley, and R. Taherian

1. Introduction

The need for accurate and convenient measurement of complex permittivities of material media cannot be overemphasized. Besides providing understanding of electromagnetic wave interaction with matter, complex permittivity information is desirable in many areas of basic and applied research in science and engineering, including process and quality control in industries, diagnostic and therapeutic applications of microwaves in biomedicine, government radiation policy formulation, characterization of reservoir rocks in bore-hole formations and prospecting in geophysical logging. Extensive work have been done in microwave measurements of complex permittivity of biological subjects, both in vivo and in vitro [1–5]. The open-ended coaxial line has been the instrument of choice in these measurements because of the nondestructive requirement. In these measurements the coaxial line is terminated by the sample material and the reflection coefficient caused

by the incident microwave signal is measured at any desired frequency. These data are then related to the complex permittivity of the sample material. The last part of the problem, i.e. relating the reflection coefficient to the complex permittivity, is not trivial and various attempts have been made to devise an accurate scheme to perform this task [6,7]. The usual procedure is to model the coaxial line and sample interface as an input impedance [8] or admittance [3,4, 9–13]. As will be shown later the input admittance model for the coaxial-sample interface is a natural result from our model. In cases where nondestructive testing is not a requirement, the coaxial line can be terminated by any convenient waveguide as sample holder. In this present work, the coaxial line is terminated with cylindrical waveguide. There are quite a few mathematical models for the coaxial line terminated in cylindrical waveguide [8,14–16]. Notable among them are the distinctive works by Risley [15,16]. Our motivation to undertake this work stems from the need to develop a full-wave general purpose model of a test cell used in experimental complex permittivity measurements of saturated reservoir rock samples. The goal of this particular measurement was to generate a complex permittivity data base for saturated reservoir rocks from bore-hole formations. We remark here that the complex permittivity of saturated reservoir formations is frequency dependent. In addition the real and imaginary parts are interdependent. The phenomenon and mechanism of this dependency are well documented in the works of Alvarez [17] and Sherman [18]. The expository works of these two reveal the inherent difficulty of interpreting complex permittivity logs without any realistic and comprehensive data base as guide.

In the next section we present an analytical model of the problem and derive the differential equations that govern electromagnetic wave propagation. Next we apply a Green's function technique to produce solutions of the magnetic fields in terms of the aperture electric field. An integral equation for the aperture electric field is solved for $zero^{th}$ order approximation and also by method-of-moments (MOM). An expression for the reflection coefficient of the incident TEM mode is derived for simulated test samples.

In section three, we accomplish the inverse problem solution via *Müller'* s method. We perform an initial error sensitivity investigation. However for a complete analytical error analyses of this method, the reader is referred to the comprehensive works of Yan-Zhen [13] and

Nyshadham [19]. Finally we apply the inverse solutions to the reflection coefficients obtained in the previous section to reconstruct the complex permittivities of the simulated samples. Plots of relative percentage error are presented to display the accuracy of the inverse solution.

The last section gives a summary of our accomplishments, draws conclusions, and gives recommendations for future work.

2. Forward Problem

The geometry of our model is depicted in Figure 1. All dimensions are given in the figure. The frequency of investigation is $1\,GHz$. The choice of our coordinate system as depicted in Figure 1 separates the problem into two distinct regions, viz: coaxial guide (coax) for $z \leq 0$ and cylindrical guide for $z \geq 0$. The regions are coupled through the aperture at $z = 0$. The coax is filled with material of dielectric constant ε_1, teflon in this case, and the cylindrical guide houses the test sample with complex permittivity ε_2. The model is excited with an azimuthally symmetric magnetic current source located at $z = -d$ in the coaxial line. Because of the azimuthal symmetry for both model geometry and excitation source, we have no ϕ-variation and our problem becomes a two-dimensional one. Furthermore, Maxwell's equations decouple into TM_z and TE_z modes with excitation limited to TM_z modes only. We assume time harmonic source with $e^{j\omega t}$ time dependence. The governing differential equations are then given by (TM_z)

$$\begin{aligned} \frac{\partial E_\rho}{\partial z} - \frac{\partial E_z}{\partial \rho} &= -j\omega\mu H_\phi - M_\phi \\ \frac{\partial H_\phi}{\partial z} &= -j\omega\varepsilon E_\rho \\ \frac{1}{\rho}\frac{\partial}{\partial \rho}(\rho H_\phi) &= j\omega\varepsilon E_z \end{aligned} \tag{1}$$

We can eliminate E_ρ and E_ϕ from the first equation of the set to obtain

$$\begin{aligned} \mathcal{L}_{\rho z} H_\phi &= j\varepsilon M_\phi \\ E_\rho &= -\frac{1}{j\omega\varepsilon}\frac{\partial H_\phi}{\partial z} \\ E_z &= \frac{1}{j\omega\varepsilon}\frac{1}{\rho}\frac{\partial}{\partial\rho}(\rho H_\phi) \end{aligned} \tag{2}$$

where

$$\mathcal{L}_{\rho z} \equiv \frac{1}{\rho}\frac{\partial}{\partial\rho}\left(\rho\frac{\partial}{\partial\rho}\right) + \frac{\partial^2}{\partial z^2} + k^2 - \frac{1}{\rho^2} \tag{3}$$

is the Laplacian in cylindriacl coordinates and $k = \sqrt{\omega^2\varepsilon\mu}$. The above set of equations govern the electromagnetic wave propagation in our model with the perfectly conducting wall assumption imposing zero tangential electric fields on the boundaries.

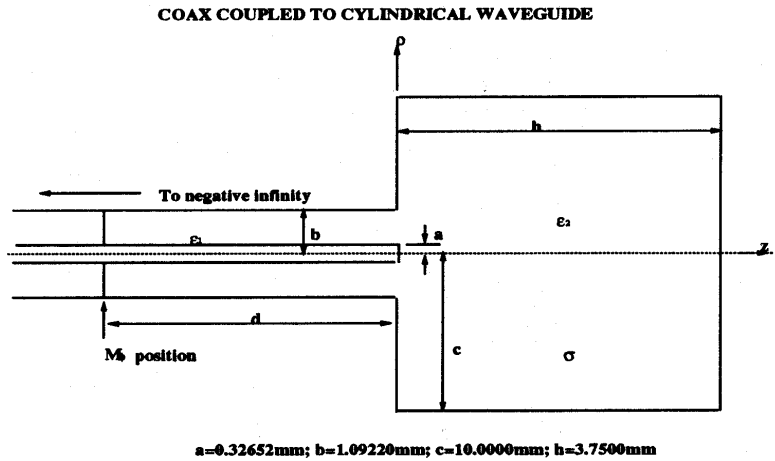

Figure 1. Coaxial waveguide coupled to cylindrical waveguide.

We now employ Greens function methods by taking the inner product of the Green's function G with the first of equations 2, to obtain in general,

$$\langle \mathcal{L}_{\rho z} H_\phi, G\rangle = \langle H_\phi, \mathcal{L}_{\rho z} G\rangle + \int_S (G\nabla H_\phi - H_\phi \nabla G)\cdot \hat{n} ds \tag{4}$$

where $\mathcal{S}$ is the surface bounding the region of interest $\mathcal{V}$, $\hat{n}$ is the unit outward normal to the surface $\mathcal{S}$ and

$$\langle \mathcal{L}_{\rho z} H_\phi, G\rangle \equiv \int_V (G\mathcal{L}_{\rho z} H_\phi) dv$$

In particular for region 1, we have

$$H_{\phi 1} = -j\omega\varepsilon \int_V G_1 M_\phi dv + \int_{\mathcal{S}} (G_1 \nabla H_{\phi 1} - H_{\phi 1} \nabla G_1) \cdot \hat{n} ds \tag{5}$$

where $H_{\phi 1}$ satisfies

$$\begin{aligned} H_{\phi 1} + \rho \frac{\partial}{\partial \rho} H_{\phi 1}\bigg|_{\rho=a,\,b} &= 0 \\ H_{\phi 1} &= H_{\phi 2} \text{ on } z = 0,\ a \le \rho \le b \\ \lim_{z \to -\infty} H_{\phi 1} &= 0 \quad \text{for } k \text{ complex} \end{aligned}$$

and for region 2, we have

$$H_{\phi 2} = \int_{\mathcal{S}} (G_2 \nabla H_{\phi 2} - H_{\phi 2} \nabla G_2) \cdot \hat{n} ds \tag{6}$$

where $H_{\phi 2}$ satisfies

$$\begin{aligned} H_{\phi 2} + \rho \frac{\partial}{\partial \rho} H_{\phi 2}\bigg|_{\rho=c} &= 0 \\ \frac{\partial}{\partial_z} H_{\phi 2}\bigg|_{z=h} &= 0 \\ \frac{\partial}{\partial_z} H_{\phi 2}\bigg|_{z=0} &= 0 \qquad \text{on } b \le \rho \le c \\ \lim_{\rho \to 0} H_{\phi 2} &\qquad \text{is finite} \end{aligned}$$

The Green's functions are chosen such that G_1 satisfies

$$\mathcal{L}_{\rho z} G_1 = -\frac{\delta(\rho - \rho')}{\rho} \delta(z - z') \tag{7}$$

$$G_1 + \rho \frac{\partial}{\partial \rho} G_1\bigg|_{\rho=a,b} = 0 \tag{8}$$

$$\begin{aligned} \frac{\partial}{\partial z} G_1\bigg|_{z=0} &= 0 \qquad (9) \\ \lim_{z \to -\infty} G_1 &= 0 \qquad \text{for } k \text{ complex} \end{aligned}$$

and G_2 satisfies

$$\mathcal{L}_{\rho z} G_2 = -\frac{\delta(\rho - \rho')}{\rho}\delta(z - z') \tag{10}$$

$$G_2 + \rho\frac{\partial}{\partial\rho}G_2\bigg|_{\rho=c} = 0 \tag{11}$$

$$\frac{\partial}{\partial z}G_2\bigg|_{z=0,h} = 0$$

$$\lim_{\rho\to 0} G_2 \qquad \text{is finite}$$

We note that the surface integrals in the solution for the magnetic fields has no contributions from the radial surfaces since

$$(G_1\nabla H_\phi - H_\phi\nabla G_1)\cdot\hat{n} = G_1\frac{\partial}{\partial\rho}H_\phi - H_\phi\frac{\partial}{\partial\rho}G_1 = \frac{G_1 H_\phi}{\rho} - \frac{G_1 H_\phi}{\rho} = 0$$

where we have applied equation 8 and 11 and also $\hat{n} = \hat{\rho}$ on the radial surface. The Green's function problems are displayed in Figure 2. When we apply the Green's functions as defined above to the magnetic field solutions the expressions become

$$H_{\phi 1} = -j\omega\varepsilon_1 M_0\int_a^b G_1(\rho, z, \rho', -d)d\rho' - j\omega\varepsilon_1\int_a^b G_1(\rho, z, \rho', 0)E_a(\rho')d\rho' \tag{12}$$

$$H_{\phi 2} = j\omega\varepsilon_2\int_a^b G_2(\rho, z, \rho', 0)E_a(\rho')d\rho' \tag{13}$$

where E_a is the radial aperture electric field, defined by

$$E_\rho|_{z=0} = -\frac{1}{j\omega\varepsilon}\frac{\partial H_\phi}{\partial z}\bigg|_{z=0} = E_a$$

and

$$M_\phi = M_o\frac{\delta(z+d)}{\rho}$$

We solve the Green's problem by seeking eigenfunction expansion in the ρ and a standard Green's function solution in the z. We let

$$G_1 = \sum_{n=0}^{\infty}\alpha_n(z)\mathcal{B}_1(\gamma_n\rho) \tag{14}$$

where $\mathcal{B}_1(\gamma_n\rho) = J_1(\gamma_n\rho)Y_0(\gamma_n a) - Y_1(\gamma_n\rho)J_0(\gamma_n a)$ and $\alpha_n(z)$ satisfies a second order ordinary differential equation which can be solved by standard Green's function methods [20]. Imposing the boundary conditions at $\rho = a,\, b$ on G_1 defines the characteristic equation

$$\frac{Y_0(\gamma_n a)}{J_0(\gamma_n a)} = \frac{Y_0(\gamma_n b)}{J_0(\gamma_n b)} \tag{15}$$

from which γ_n 's are determined. A complete solution for G_1 is then obtained as

$$G_1(\rho,\, z,\, \rho',\, z') = \frac{-j}{k_1\rho\rho' \ln(b/a)} \begin{cases} e^{jk_1 z'}\, \cos(k_1 z) & ;z > z' \\ e^{jk_1 z}\, \cos(k_1 z') & ;z < z' \end{cases} \tag{16}$$

for $n = 0$ and

$$G_1(\rho,\, z,\, \rho',\, z') = -\sum_{n=1}^{\infty} \left(\frac{\mathcal{B}_1(\gamma_n\rho)\mathcal{B}_1(\gamma_n\rho')}{\frac{2}{(\pi\gamma_n)^2}\left[\frac{J_0^2\gamma_n a)}{J_0^2(\gamma_n b)} - 1\right]} \right) \frac{j}{k_{1n}} \begin{cases} e^{jk_{1n} z'}\, \cos(k_{1n} z) & ;z > z' \\ e^{jk_{1n} z}\, \cos(k_{1n} z') & ;z < z' \end{cases} \tag{17}$$

otherwise. We note also that $k_{1n}^2 = k_1^2 - \gamma_n^2$.

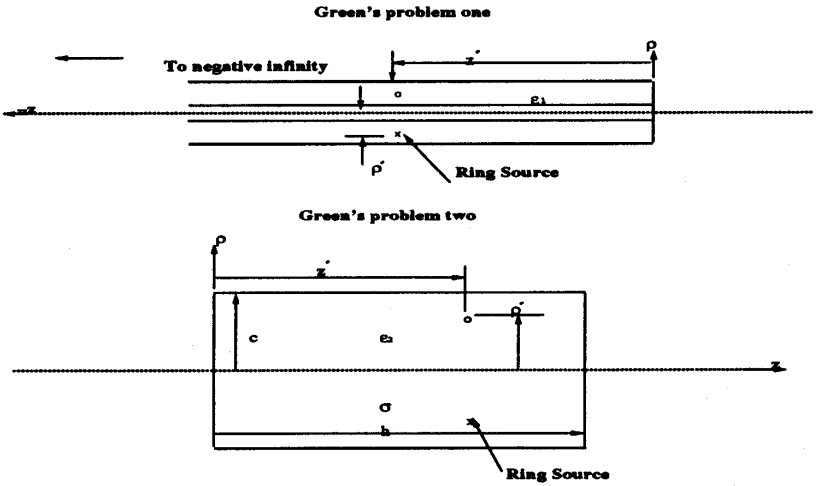

Figure 2. Green's problems.

Similarly we choose G_2 as

$$G_2 = \sum_{n=1}^{\infty} J_1(\lambda_n\rho) S_n(z) \tag{18}$$

and obtain its solution as

$$G_2(\rho,z,\rho',z') = -\sum_{n-1}^{\infty} \frac{2J_1(\lambda_n\rho')J_1(\lambda_n\rho)}{c^2J_1^2(\lambda_n c)k_{2n}\sin(k_{2n}h)} \times \begin{cases} \cos(k_{2n}z)\cos[k_{2n}(h-z')] & z<z' \\ \cos(k_{2n}z')\cos[k_{2n}(h-z)] & z>z' \end{cases} \tag{19}$$

where $J_0(\lambda_n c) = 0$ is the characteristic function for determining λ_n's and $k_{2n}^2 = k_2^2 - \lambda_n^2$. This completes the formal solutions to the Green's function problems. It is instructive to note that this is only one of many possible forms of solution. We could as well have produced solutions using eigenfunctions in the z-domain instead of the ρ-domain or eigenfunctions in both domains. The particular form adopted here is conducive to the numerical computations for the problem at hand.

When we incorporate the Green's function solutions into the H_ϕ expressions and perform the integration over the source term, the results are

$$H_{\phi 1} = -\frac{\omega\varepsilon_1}{k_1\rho} I_0\cos(k_1 z) - j\omega\varepsilon_1 \int_a^b \rho' G_1(\rho,z,\rho',0)E_a(\rho')d\rho' \tag{20}$$

$$H_{\phi 2} = j\omega\varepsilon_2 \int_a^b \rho' G_2(\rho,z,\rho',0)E_a(\rho')d\rho' \tag{21}$$

where $I_0 = M_0 e^{-jk_1 d}$ and

$$G_1(\rho,z,\rho',0) = -j\frac{1}{k_1\rho\rho'\ln(b/a)}e^{jk_1 z} - j\sum_{n=1}^{\infty}\left(\frac{\mathcal{B}_1(\gamma_n\rho)\mathcal{B}_1(\gamma_n\rho')}{k_{1n}\frac{2}{(\pi\gamma_n)^2}\left[\frac{J_0^2\gamma_n a)}{J_0^2(\gamma_n b)}-1\right]}\right)e^{jk_{1n}z}$$

$$G_2(\rho,z,\rho',0) = -\sum_{n=1}^{\infty}\frac{2J_1(\lambda_n\rho')J_1(\lambda_n\rho)}{c^2J_1^2(\lambda_n c)k_{2n}\sin(k_{2n}h)}\cos[k_{2n}(h-z)]$$

We can normalize H_ϕ by dividing through with $\omega\varepsilon_1 I_0$ to obtain

$$\bar{H}_{\phi 1} = -\frac{1}{k_1\rho}\cos(k_1 z) - j\int_a^b \rho' G_1(\rho,z,\rho',0)\bar{E}_a(\rho')d\rho' \tag{22}$$

$$\bar{H}_{\phi 2} = j\varepsilon_r \int_a^b \rho' G_2(\rho,z,\rho',0)\bar{E}_a(\rho')d\rho' \tag{23}$$

where $\varepsilon_r = \varepsilon_2/\varepsilon_1$ and $\bar{H} = (H_{\phi 1}/\omega I_0)$, etc. We shall now drop the bar with the understanding that these quantities are normalized as shown above. Next we demand continuity of the fields in the aperture, i.e, $H_{\phi 1} = H_{\phi 2}$ at $z = 0$ to produce an integral equation for E_a as

$$-\frac{1}{k_1\rho} = -j\int_a^b \rho'(G_1(\rho,0,\rho',0) + \varepsilon_r G_2(\rho,0,\rho',0))E_a(\rho')d\rho' \qquad (24)$$

The above integral equation can be solved analytically or numerically depending on the functional form assumed for E_a. In this work we present two types of solutions, a $zero^{th}$ order solution which is analytical and a numerical solution via method of moments.

2.1. Zero th order solution

We let the functional form of E_a be given by

$$E_a(\rho) = E_0\frac{1}{\rho} + \sum_{n=1}^{\infty} E_{1n}\mathcal{B}_1(\gamma_n\rho). \qquad (25)$$

where E_0 and E_{1n} are modal constants. In the $zero^{th}$ order solution we assume a dominant TEM model and approximate E_z by E_o/ρ. Substituting this approximation into the integral equation allows us to perform the ρ' integration immediately, to give

$$-\frac{1}{k_{1\rho}} = E_0\frac{1}{k_1\rho} + j2\varepsilon_r E_0\sum_{n=1}^{\infty}\left(\frac{J_0(\lambda_n b) - J_0(\lambda_n a)}{c^2\lambda_n J_1^2(\lambda_n c)k_{2n}\tan(k_{2n}h)}\right)J_1(\lambda_n\rho) \qquad (26)$$

Integrating equation 26 on ρ from a to b yields an average value for E_0 as

$$E_0 = -1\Bigg/\left(1 - j^2\varepsilon_r\frac{1}{\ln(b/a)}\sum_{n=1}^{\infty}\frac{(J_0(\lambda_n b) - J_0(\lambda_n a))^2}{c^2\lambda_n^2 J_1^2(\lambda_n c)k_{2rn}\tan(k_{2n}h)}\right) \qquad (27)$$

where $k_{2rn} = k_{2n}/k_1$. Equation 27 can be evaluated numerically to obtain an approximation for E_a. Higher order approximations for E_a could be obtained by taking more terms in equation 25. Indeed using the full expression in equation 25 is the usual modal expansion solution as it is known in the literature. However we prefer the method of moments solution presented next.

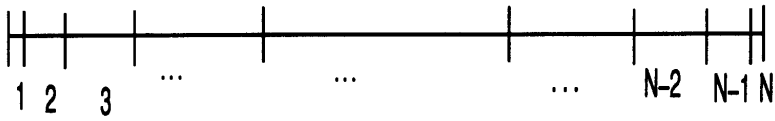

Figure 3. Aperture subintervals

2.2. Method of moments

We begin by partitioning the aperture into N subintervals as shown in Figure 3. We progressively refine the subintervals intervals towards both edges in other to simulate the edge-singularity of the aperture field while limiting the number of unknowns. We define the subintervals starting from $\rho = a$ as

$$\Delta_{p+1} = \binom{N-1}{p}^m \Delta$$

$$\binom{N-1}{p} = \frac{(N-1)!}{(N-p-1)!p!}$$

$$\Delta = (b-a) \Big/ \sum_{p=0}^{N-1} \binom{N-1}{p}^m$$

where m is an edge refining factor. Increasing m refines the subintervals at the edges. In this particular work, $m = 2$ in all results presented. We next approximate the aperture electric field E_a with a set of pulse functions defined by

$$E_a(\rho) = \sum_{n=1}^{N} e_p \frac{f_p(\rho)}{\rho} \tag{28}$$

$$f_p(\rho) = \begin{cases} 1 & \text{on } p^{th} \text{ subinterval} \\ 0 & \text{otherwise} \end{cases} \tag{29}$$

When we insert, $E_a(\rho)$ as defined in 28 into the integral equation, we obtain

$$-\frac{1}{k_1 \rho} = j \sum_{n=1}^{N} e_p \int^{\Delta_p} \rho'(G_1(\rho, \rho') + \varepsilon_r G_2(\rho, \rho'))d\rho' \tag{30}$$

where the integration is restricted only to the p^{th} element. In order to avoid the instabilities due to the edge singularities, we apply delta

weighting functions given by

$$W_q(\rho) = \frac{\delta(\rho - \rho_q)}{\rho} \tag{31}$$

where ρ_q is the midpoint of the q^{th} element. An inner product of equation 30 with W_q yields

$$-\frac{1}{k_1\rho_q} = j\sum_{n=1}^{N} e_p \int^{\Delta_p} \rho'(G_1(\rho_q,\rho') + \varepsilon_r G_2(\rho_q,\rho'))d\rho' \tag{32}$$

which is an $N \times N$ matrix equation. An explicit expression for equation 32 is

$$\begin{aligned}\frac{1}{k_1\rho_q} = &-\frac{1}{k_1\rho_q}\sum_{p=1}^{N} e_p\left(\frac{\ln(\rho_p/\rho_{p-1})}{\ln(b/a)}\right)\\ &+\frac{1}{2}\pi^2\sum_{p=1}^{N} e_p\left\{\sum_{n=1}^{\infty}\frac{\gamma_n}{k_{1n}}\left(\frac{\mathcal{B}_1(\gamma_n\rho_q)[\mathcal{B}_o(\gamma_n\rho_p)-\mathcal{B}_0(\gamma_n\rho_{p-1})]}{\left[\frac{J_0^2(\gamma_n a)}{J_0^2(\gamma_n b)}-1\right]}\right)\right\}\\ &-j2\varepsilon_r\sum_{p-1}^{N} ep\left\{\sum_{n=1}^{\infty}\left(\frac{J_1(\lambda_n\rho_q)[J_0(\lambda_n\rho_p)-J_0(\lambda_n\rho_{p-1})]}{c^2\lambda_n k_{2n}J_1^2(\lambda_n c)(\tan(k_{2n}h)}\right)\right\}\end{aligned} \tag{33}$$

This completes the general N - *element* method of moments solution. Specializing the above result to $N = 1$, we obtain

$$\frac{1}{k_1\rho_q} = -\frac{1}{k_1\rho_q}e_1 - j2\varepsilon_r e_1\sum_{n=1}^{\infty}\left(\frac{J_1(\lambda_n\rho_q)[J_0(\lambda_n b)-J_0(\lambda_n a)]}{c^2\lambda_n k_{2n}J_1^2(\lambda_n c)\tan(k_{2n}h)}\right) \tag{34}$$

where $\rho_q = (a+b)/2$. Results presented later will show that using one element $(N = 1)$ is sufficient to obtain reasonable accuracy in the reconstruction. We therefore restrict the solutions in all cases except for E_a computation, to $zero^{th}$ order and the one-element method of moments.

2.3. Asymptotic analysis

This section considers asymptotic techniques that aid in an efficient computation of the matrix coefficients in equation 33 and 34

above. An attempt to evaluate these matrix coefficients directly is inefficient. This is a consequence of the oscillatory behavior of *Bessel's* functions. The method we propose here exploits the rapid rate at which *Bessel's* functions approach their asymptotic limits. The technique [22] is to find the asymptotic limit of the individual terms in the summation with the hope that we can sum the series of the asymptotic limits into an analytical closed form expression. Then we only need to add the difference between each individual term and the asymptotic limit to the closed form expression obtained. Because of the rate at which these terms approach their asymptotic limits, only a few terms are needed in the difference computation for accuracies of practical interest. We begin by finding the asymptotic limits of the various terms in equation 33 as follows:

$$\lim_{n\to\infty} \lambda_n = \frac{\pi}{c}(n - 1/4) \tag{35}$$

$$\lim_{n\to\infty} \gamma_n = \frac{\pi n}{(b-a)} \tag{36}$$

$$\lim_{n\to\infty} \left(\frac{J_0^2(\gamma_n a)}{J_0^2(\gamma_n b)} - 1 \right) = \left(\frac{b}{a} \right) - 1 \tag{37}$$

Since most of the asymptotic limits can be derived by direct substitution, we will only quote the results. It is convenient to note the simple form of these asymptotic limits of such seemingly complicated functions. These simple asymptotic forms are instrumental in the success of this method. The asymptotic forms of the various terms in the matrix equation are:

$$\lim_{n\to\infty} \left(\frac{2J_1(\lambda_n\rho_q)J_0(\lambda_n\rho_q)}{c^2\lambda_n k_{2n} J_1^2(\lambda_n c)\tan(k_{2n}h)} \right) = c\frac{\cos(\theta_2(n-\frac{1}{4})) + \sin(\theta_1(n-\frac{1}{4}))}{2\pi^2(n-\frac{1}{4})^2\sqrt{\rho_q\rho_p}} \tag{38}$$

$$\lim_{n\to\infty} \frac{\gamma_n}{k_{1n}} \left(\frac{\mathcal{B}_1(\gamma_n\rho_q)\mathcal{B}_0(\gamma_n\rho_p)}{\frac{2}{(\pi\gamma_n)^2}\left[\frac{J_0^2(\gamma_n a)}{J_0^2(\gamma_n b)} - 1\right]} \right) = -j\frac{4q(\frac{b}{a}-1)}{\pi^4 n^2\sqrt{\rho_q\rho_p}} \cos(n\psi_1)\sin(n\psi_2) \tag{39}$$

$$\theta_1 = \frac{\pi}{c}(\rho_p - \rho_q)$$
$$\theta_2 = \frac{\pi}{c}(\rho_q + \rho_p)$$
$$\psi_1 = \pi \left(\frac{\rho_q}{a} - 1\right) \Big/ \left(\frac{b}{a} - 1\right)$$
$$\psi_2 = \pi \left(\frac{\rho_p}{a} - 1\right) \Big/ \left(\frac{b}{a} - 1\right)$$

We remark that even though these result are derived for n approaching infinity, the difference between theses limits and exact terms is already of order 10^{-3} for $n = 2$. In order to exploit fully these simple asymptotic forms, we must be able to find closed form or rapidly converging expressions for the following infinite series:

$$\sum_1^\infty \frac{e^{j(n\theta)}}{n^2}$$
$$\sum_1^\infty \frac{e^{j(n-\alpha)\theta}}{(n-\alpha)^2} \tag{40}$$

This is possible for the first series [21, 24]. In case of the second series, we are not aware of any useful expressions except for the special case when $\alpha = 1/2$. However, we can improve their convergence by writing

$$\frac{1}{(n-\alpha)^2} \text{ as } \frac{1}{n^2} + \frac{\alpha}{n^3} + \frac{3\alpha^2}{n^2(n-\alpha)^2} - \frac{2\alpha^3}{n^3(n-\alpha)^2}$$

The process produces series of the first type and accelerates the convergence from n^{-2} to n^{-4}. Further increase in the rate of convergence can be achieved by extending this process to higher orders. However to what extent, becomes a choice between mathematical complexity and computational expediency. The closed form or rapidly converging expressions for the various series employed in the analysis are given below as:

$$\sum_1^\infty \frac{\sin(n\theta)}{n^2} = -\left(\theta \ln\theta - \theta + \sum_1^\infty \frac{|\mathcal{B}_{2n}|\theta^{2n+1}}{2n(2n+1)!}\right)$$
$$\sum_1^\infty \frac{\sin(n\theta)}{n^3} = \frac{\pi^2}{6}\theta - \frac{\pi}{4}\theta^2 + \frac{1}{12}\theta^3$$
$$\sum_1^\infty \frac{\sin(n\theta)}{n^4} = \zeta(3)\theta + \frac{1}{6}\theta^3 \ln(\theta) - \frac{11}{36}\theta^3 + \sum_1^\infty \frac{|\mathcal{B}_{2n}|\theta^{2n+1}}{2n(2n+3)!}$$

$$\sum_{1}^{\infty}\frac{\cos(n\theta)}{n^2} = \frac{\pi^2}{6} - \frac{\pi}{2}\theta + \frac{1}{4}\theta^2$$

$$\sum_{1}^{\infty}\frac{\cos(n\theta)}{n^3} = \zeta(3) + \frac{1}{2}\theta^2\ln(\theta) - \frac{3}{4}\theta^2 + \sum_{1}^{\infty}\frac{|\mathcal{B}_{2n}|\theta^{2n+2}}{2n(2n+2)!}$$

$$\sum_{1}^{\infty}\frac{\cos(n\theta)}{n^4} = \frac{\pi^4}{90} - \frac{\pi^4}{12}\theta^2 + \frac{\pi}{12}\theta^2 - \frac{1}{48}\theta^4$$

where B_m and $\zeta(x)$ are the *Bernoulli-Euler* number and *Riemann Zeta* functions respectively. The mechanics of the computation process is to subtract from the individual terms in the series, the asymptotic limits, sum the resulting difference series and then add the summations of the asymptotic series. The net effect is accelerated convergence. Symbolically, the above process can be described as

$$\sum_{1}^{\infty}(T_n) = \sum_{1}^{\infty}(T_n - T_{lim}) + T_{lim-sum} \tag{41}$$

where T_n is the N^{th} term in the series, $T_{lim} = \lim_{n\to\infty} T_n$ and $T_{lim-sum} = \sum_{1}^{\infty}(T_{lim})$. Figure 4 shows the plots of E_a for different number of elements. We note the well defined edge singularities of the aperture electric field E_a. In the next section we derive expressions for the reflection coefficient of the incident *TEM* mode.

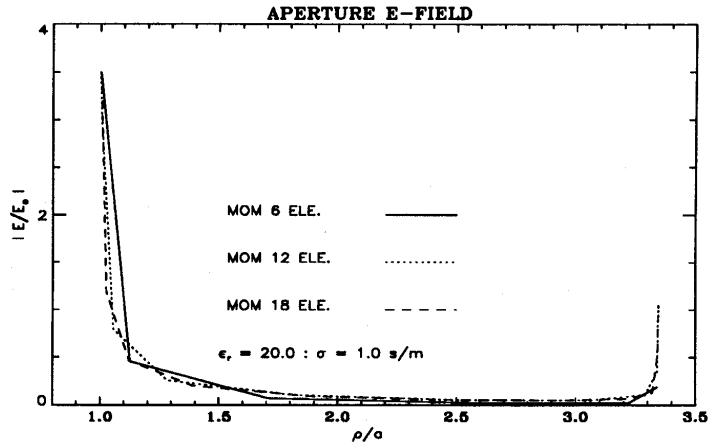

Figure 4. Effect of number of elements on aperture electric field: $a = 0.32652mm$, $b = 1.0922mm$, $c = 10.000mm$, $h = 37.5mm$, $\sigma = 1.0s/m$, $\varepsilon_r = 20.00$.

2.4. Reflection coefficient

One of the most important scattering parameters in microwave measurements is the reflection coefficient. In this section we derive an expression for the *TEM* mode reflection coefficient in the coaxial waveguide. We can rewrite $H_{\phi 1}$ as

$$H_{\phi 1}(\rho,z) = -\frac{1}{2k_1\rho}\left[e^{-jk_1 z} + \left(1 + \frac{2}{\ln(b/a)}\int_a^b E_a(\rho')d\rho\right)e^{jk_1 z}\right] - j\sum_{n=1}^{\infty}\left(\frac{\mathcal{B}_1(\gamma_n\rho)}{\frac{2}{(\pi\gamma)n)^2}\left[\frac{J_0^2(\gamma_n a)}{J_0^2(\gamma_n b)} - 1\right]}\right)e^{jk_{1n}z}\int_a^b \mathcal{B}(\gamma_n\rho')E_a(\rho')d\rho'. \tag{42}$$

When $H_{\phi 1}$ is written in terms of the electric field *TEM* mode reflection coefficient, i.e.

$$H_{\phi 1}(\rho,z) = -\frac{1}{2k_1\rho}(e^{-jk_1 z} - \Gamma e^{jk_1 z}) - j\sum_{n=1}^{\infty}\left(\frac{\mathcal{B}_1(\gamma_n\rho)}{\frac{2}{(\pi\gamma_n)^2}\left[\frac{J_0^2(\gamma_n a)}{J_0^2(\gamma_n b)} - 1\right]}\right)e^{jk_{1n}z}\int_a^b \mathcal{B}(\gamma_n\rho')E_a(\rho')d\rho'. \tag{43}$$

the reflection coefficient Γ for the *TEM* mode is readily identified as

$$\Gamma = -\left(1 + \frac{2}{\ln(b/a)}\int_a^b E_a(\rho')d\rho'\right) \tag{44}$$

Generalizing this concept, we may express $H_{\phi 1}(\rho,z)$ as

$$H_{\phi 1}(\rho,z) = -\frac{1}{ak_1\rho}(e^{-jk_1 z} - \Gamma e^{jk_1 z}) - \sum_{n=1}^{\infty} f_n(\rho)\Gamma_n e^{jk_{1n}z} \tag{45}$$

where Γ_n and $f_n(\rho)$ are defined as

$$\left(\frac{j}{\frac{2}{(\pi\gamma_n)^2}\left[\frac{J_0^2(\gamma_n a)}{J_0^2(\gamma_n b)} - 1\right]}\right)\int_a^b \mathcal{B}_1(\gamma_n\rho')E_a(\rho')d\rho \tag{46}$$

and

$$\mathcal{B}_1(\gamma_n\rho) \tag{47}$$

respectively. The Γ_n 's are the reflection coefficients of the higher order modes generated in the aperture. These evanescent higher order modes are restricted mainly to the immediate neighborhood of the aperture. Explicit expressions of Γ for the $zero^{th}$ and MOM solutions are

$$\Gamma = -(1 + 2E_0) \tag{48}$$

and

$$\Gamma = -\left[1 + \frac{2}{\ln(b/a)} \sum_{p=1}^{N} e_p \ln\left(\frac{\rho_p}{\rho_p - 1}\right)\right] \tag{49}$$

respectively. Even though the reflection coefficient is defined for the coaxial waveguide TEM mode, the solution contains a superpositon of all the higher order modes generated in the aperture. A reflection coefficient contour plot of some text samples is shown in Figure 5. As expected, the magnitude of the reflection coefficient varies inversely with conductivity and directly with dielectric constant at low conductivities. This is due to greater energy dissipation at higher conductivities and higher energy propagation for larger values of dielectric constants. But at very high conductivities, the magnitude of the reflection coefficient increases with conductivity. This is because at very high conductivities, the aperture appears as a short to the incident wave. We note in later plots that the guide resonates for text samples with relative dielectric constant (ϵ_r) values of 63 and 70 approximately. Figure 6 displays the same information in figure 5 using a $zero^{th}$ order approximation.

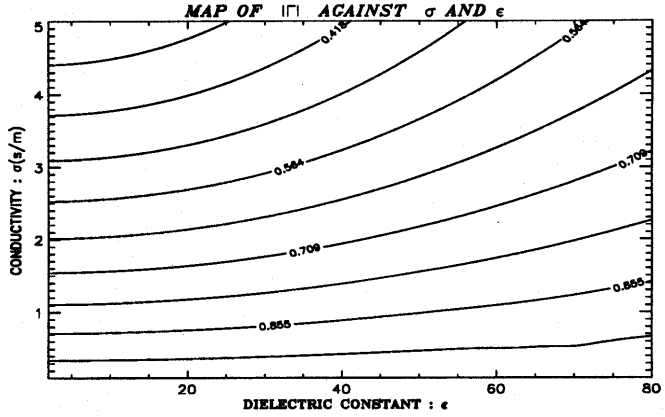

Figure 5. Contour map of reflection coefficient of simulated test samples for 1 - *element* **MOM:** $a = 0.32652mm$, $b = 1.0922mm$, $c = 10.000mm$, $h = 37.5mm$.

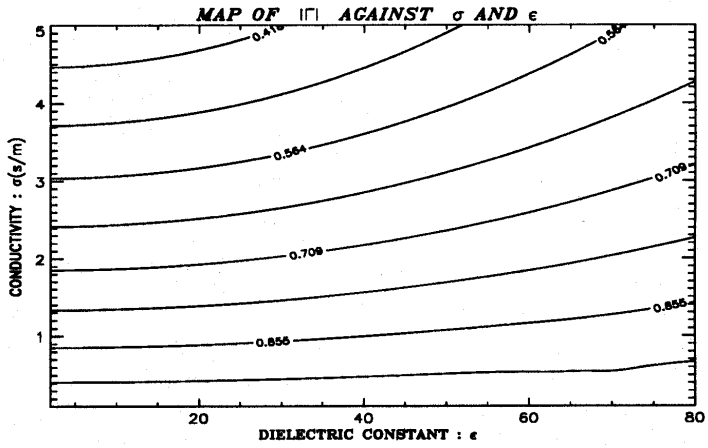

Figure 6. Contour map of reflection coefficient of simulated test samples for $zero^{th}$ **order:** $a = 0.32652mm$, $b = 1.0922mm$, $c = 10.000mm, h = 37.5mm$.

For a cylindrical cavity the TM and TE resonant frequencies are define respectively by

$$(f_r)_{npq}^{TM} = \frac{1}{2\pi c\sqrt{\epsilon\mu}}\sqrt{\lambda_{np}^2 + \left(\frac{q\pi c}{h}\right)} \tag{50}$$

$$(f_r)_{npq}^{TE} = \frac{1}{2\pi c\sqrt{\epsilon\mu}}\sqrt{\lambda_{np}'^2 + \left(\frac{q\pi c}{h}\right)} \tag{51}$$

where c is the cylinder radius, h is the height, λ_{np} is the p^{th} root of $J_n(\lambda c)$ and λ'_{np} is the p^{th} root of $J'_n(\lambda c)$. Numerical computations show the cavity resonates at $(f_r)_{010}^{TM} = 1.0GHz$ for dielectric constant (ϵ_r) value of 62.70 and $(f_r)_{011}^{TM} = 1.0GHz$ for dielectric constant (ϵ_r) value of 70.31. These values agree very well with resonant points observed form later plots in the inverse problem.

The quality factor Q which is defined by

$$Q = \frac{\omega \times \text{energy stored}}{\text{average power dissipated}} \tag{52}$$

reduces in case of dielectric losses only to

$$Q = \frac{\omega\epsilon' \int\int\int |E|^2 dr}{\omega\epsilon'' \int\int\int |E|^2 dr} = \frac{\epsilon'}{\epsilon''} \tag{53}$$

where ϵ' and ϵ'' are the real and imaginary parts of the complex permittivity. High Q's, which signal well defined resonant points imply that resonant points can be observed at low σ and high ϵ_r.

3. Inverse Problem

In this section we produce a formulation for the inverse problem based on *Müller's* method [23]. This is then applied to the reflection coefficients from the forward problem to reconstruct sample complex permittivities. The concept is to approximate a nonlinear function $f(x) = 0$ with a quadratic function $ax^2 + bx + c$ by the Lagrangian interpolation formula. A solution is accomplished by locating the *zero*'s of $f(x)$ using a variation of the standard quadratic formula. From earlier expression for the *TEM* mode reflection coefficient, we derive expression for normalized aperture input admittance Y_0 for the $zero^{th}$ order as

$$Y_0 = -j2\epsilon_r \frac{1}{\ln(b/a)} \sum_{n=1}^{\infty} \frac{(J_0(\lambda b) - J_0(\lambda_n a))^2}{c^2 \lambda_n^2 J_1^2(\lambda_n c) k_{2rm} \tan(k_{wn} h)} \tag{54}$$

where k_{2rn} and k_{2n} are function of ε_r and the normalized aperture input admittance is defined by

$$Y = \frac{1 - \Gamma}{1 + \Gamma}$$

In the case of *1 - element MOM*, we obtain

$$Y_1 = j2\varepsilon_r \rho_q \sum_{n=1}^{\infty} \frac{(J_0(\lambda_n b) - J_0(\lambda_n a)) J_1(\lambda_n (a-b)/2)}{c^2 \lambda_n J_1^2(\lambda_n c) k_{2rn} \tan(k_{2n} h)}. \tag{55}$$

In order to apply *M̈ller's* formula we define an implicit function $f(\varepsilon_r)$ for ε_r such that $f(\varepsilon_r) = 0$. The root of $f(\varepsilon_r)$ then yields the complex permittivity of the medium. For the $zero^{th}$ order $f(\varepsilon_r)$ is given by

$$f(\varepsilon_r) = -Y_0 - j2\varepsilon_r \frac{1}{\ln(b/a)} \sum_{n=1}^{\infty} \frac{(J_0(\lambda b) - J_0(\lambda_n a))^2}{c^2 \lambda_n^2 J_1^2(\lambda_n c) k_{2rn} \tan(k_{2n} h)} \tag{56}$$

or

$$f(\varepsilon_r) = \frac{\Gamma - 1}{\Gamma + 1} - j2\varepsilon_r \frac{1}{\ln(b/a)} \sum_{n=1}^{\infty} \frac{(J_0(\lambda b) - J_0(\lambda_n a))^2}{c^2 \lambda_n^2 J_1^2(\lambda_n c) k_{2rn} \tan(k_{2n} h)} \quad (57)$$

A similar expression derived for the 1 - *element MOM* is

$$f(\varepsilon_r) = -Y_1 + j2\varepsilon_r \rho_q \sum_{n=1}^{\infty} \frac{(J_0(\lambda_n b) - J_0(\lambda_n a)) J_1(\lambda_n (a-b)/2)}{c^2 \lambda_n J_1^2(\lambda_n c) k_{2rn} \tan(k_{2n} h)}. \quad (58)$$

or

$$f(\varepsilon_r) = \frac{\Gamma - 1}{\Gamma + 1} + j2\varepsilon_r \rho_q \sum_{n=1}^{\infty} \frac{(J_0(\lambda_n b) - J_0(\lambda_n a)) J_1(\lambda_n (a-b)/2)}{c^2 \lambda_n J_1^2(\lambda_n c) k_{2rn} \tan(k_{2n} h)}. \quad (59)$$

Figure 7 and 8 show relative errors in 1 - *element* MoM reconstruction of simulated samples from reflection coefficients of the forward problem We observe a high degree of accuracy except near resonant points at ϵ_r values of 63 and 70 approximately. Figures 9 and 10 are surface plots of the same data for Figures 7 and 8 respectively. Figures 11 through 14 are the $zero^{th}$ order versions of Figures 7 through 10 respectively.

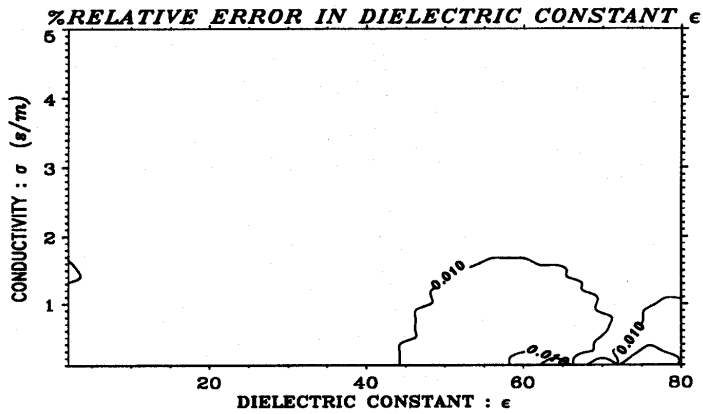

Figure 7. Contour map of reflection coefficient percent relative error in dielectric constants reconstruction for 1 - *element* MoM: $a = 0.32652mm, b = 1.0922mm,\ c = 10.000mm, h = 37.5mm.$

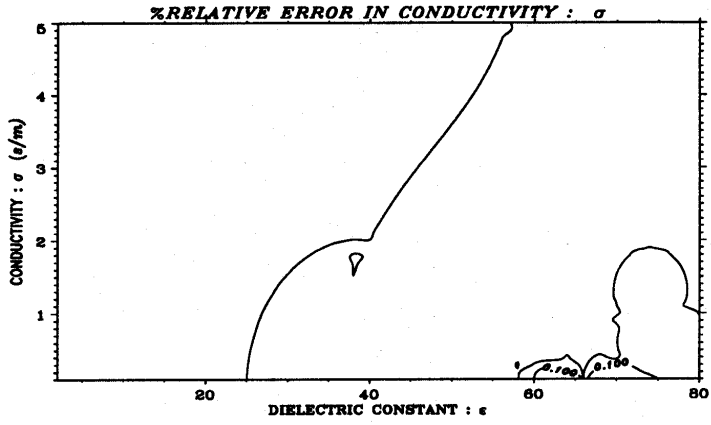

Figure 8. Contour map of reflection coefficient percent relative error in conductivities reconstruction for 1 - *element* **MoM:** $a = 0.32652mm, b = 1.0922mm,\ c = 10.000mm, h = 37.5mm.$

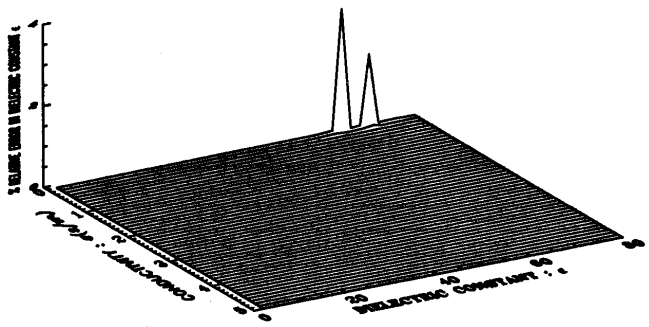

Figure 9. Relief map of percent relative error in dielectric constants reconstruction for 1 - *element* **MoM:** $a = 0.32652mm, b = 1.0922mm,\ c = 10.000mm, h = 37.5mm.$

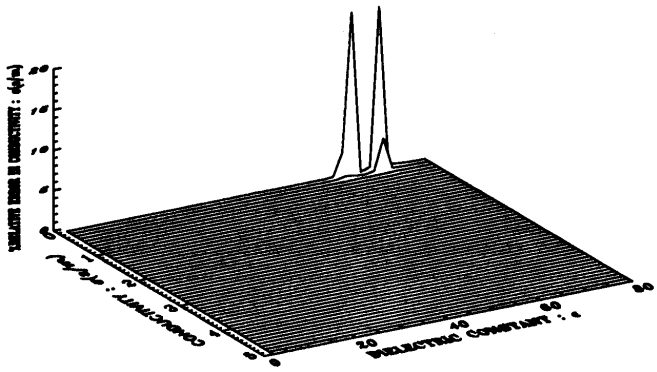

Figure 10. Relief map of percent relative error in conductivities reconstruction for 1 - *element* **MoM:** $a = 0.32652mm, b = 1.0922mm, c = 10.000mm, h = 37.5mm.$

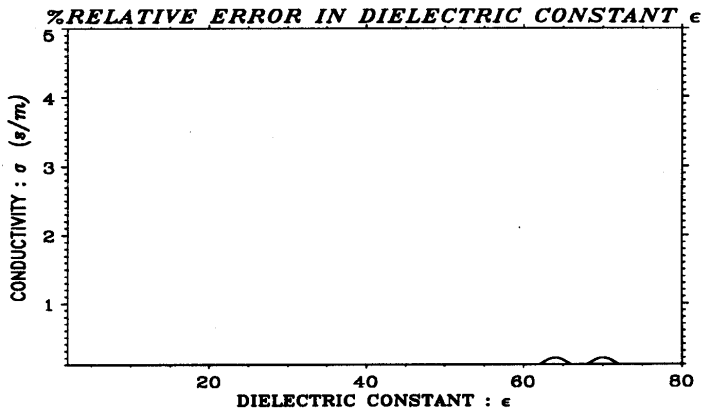

Figure 11. Contour map of percent relative error in dielectric constants reconstruction for $zero^{th}$ **order:** $a = 0.32652mm, b = 1.0922mm, c = 10.000mm, h = 37.5mm.$

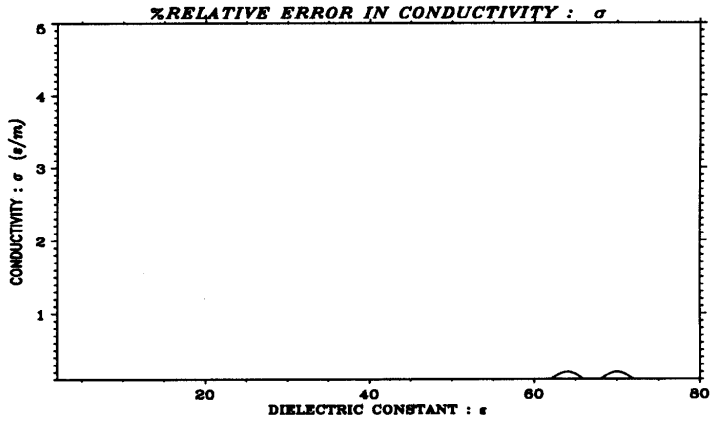

Figure 12. Contour map of percent relative error in conductivities reconstruction for $zero^{th}$ order: $a = 0.32652mm, b = 1.0922mm, c = 10.000mm, h = 37.5mm$

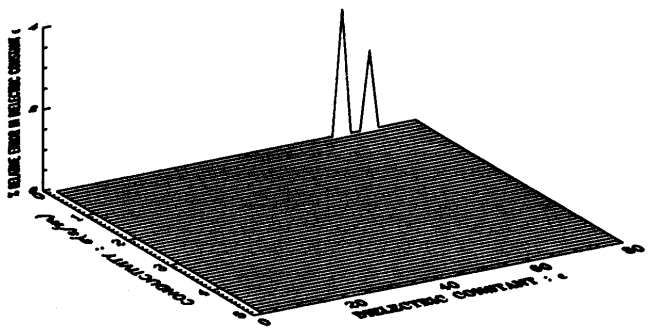

Figure 13. Relief map of percent relative error in dielectric constants reconstruction for $zero^{th}$ order: $a = 0.32652mm, b = 1.0922mm, c = 10.000mm, h = 37.5mm$

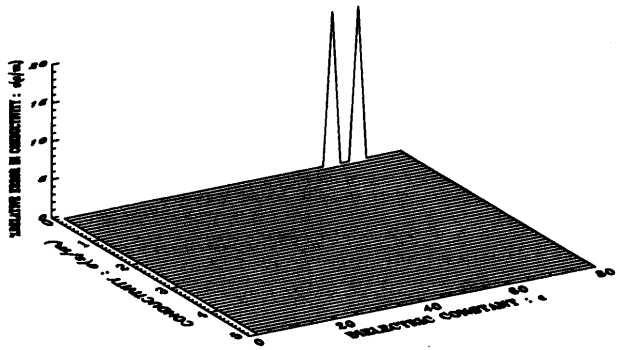

Figure 14. Relief map of percent relative error in conductivities reconstruction for $zero^{th}$ **order:** $a = 0.32652mm, b = 1.0922mm, c = 10.000mm, h = 37.5mm$

3.1. Noise sensitivity

We have performed error (noise) sensitivity by contaminating the input data. In order to quantize the accumulative effect of the input uncertainties [7] for the inverse problem, uniformly generated random errors are superimposed on the computed Γ's. We let α be the maximum random error, and Γ_{max} the maximum of the magnitude of the Γ's. Then we impose a limit on the α such that

$$x\% \geq x_{min}\% = \tau \frac{\alpha}{\Gamma_{max}} \times 100 \tag{60}$$

where τ is a scaling factor for the generated random noise and x_{min} is a chosen percentage limit relative to Γ_{max}. We note that with reference to the minimum of the magnitude of Γ, the percentage noise imposed will be greater than $x_{min}\%$. The maximum noise introduced therefore is bounded by

$$x\% \leq x_{max}\% = \tau \frac{\alpha}{\Gamma_{min}} \times 100 \tag{61}$$

where τ is computed from equation 60. Figures 15 through 22 represent the same information in Figures 7 through 14 but with contaminated input data. We observe higher values of relative errors in ϵ_r reconstruction at high conductivities and in σ reconstruction at high dielectric constants. We also note noise attenuation in ϵ_r reconstruction and noise amplification in σ reconstruction from these plots.

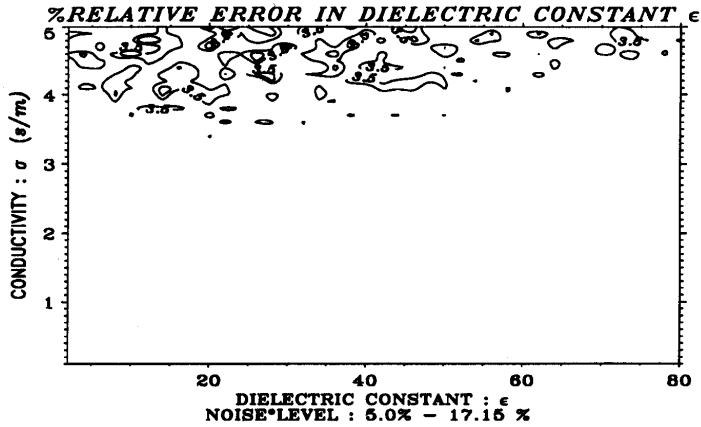

Figure 15. Contour map of percent relative error in dielectric constants reconstruction for 1 - *element* **MoM:** $a = 0.32652mm, b = 1.0922mm$, $c = 10.000mm$, $h = 37.5mm$, $(x_{min}\% - x_{max}\%)$.

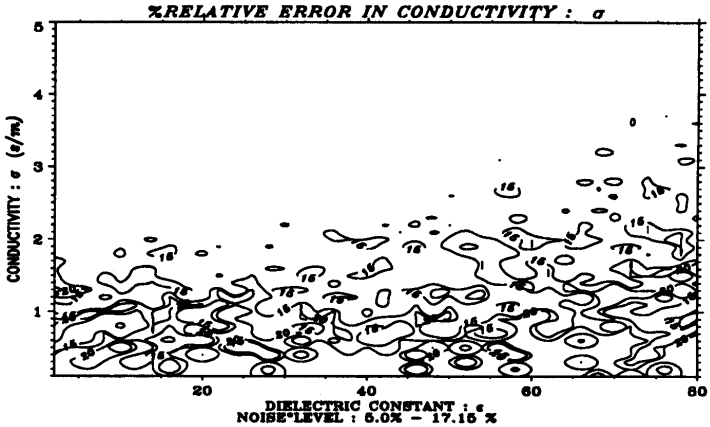

Figure 16. Contour map of percent relative error in conductivities reconstruction for 1 - *element* **MoM:** $a = 0.32652mm, b = 1.0922mm$, $c = 10.000mm, h = 37.5mm$

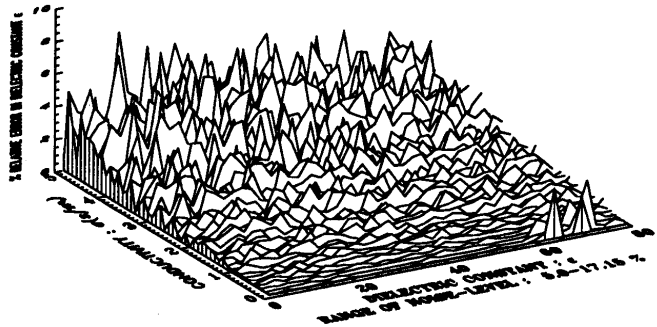

Figure 17. Relief map of percent relative error dielectric constants reconstruction for 1 - *element* **MoM:** $a = 0.32652mm, b = 1.0922mm$, $c = 10.000mm, h = 37.5mm$, $(x_{min}\% - x_{max}\%)$

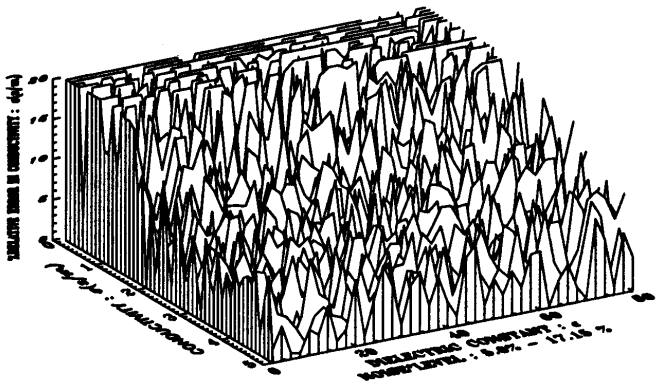

Figure 18. Relief map of percent relative error in conductivities reconstruction for 1 - *element* **M0M:** $a = 0.32652mm, b = 1.0922mm$, $c = 10.000mm, h = 37.5mm$, $(x_{min}\% - x_{max}\%)$

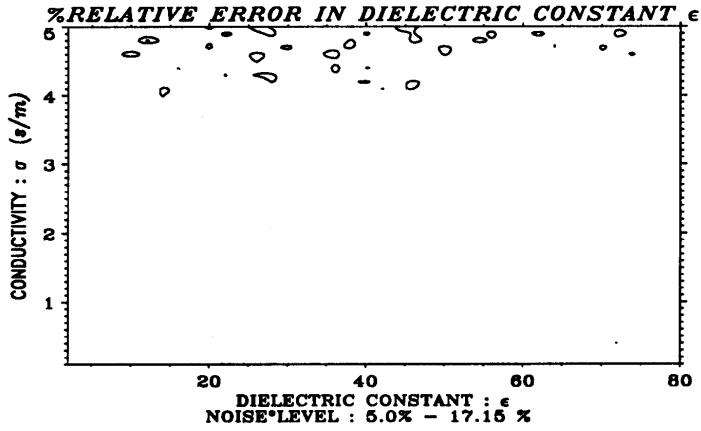

Figure 19. Contour map of percent relative error in dielectric constants reconstruction for $zero^{th}$ **order:** $a = 0.32652mm, b = 1.0922mm, c = 10.000mm$, $h = 37.5mm(x_{min}\% - x_{max}\%)$

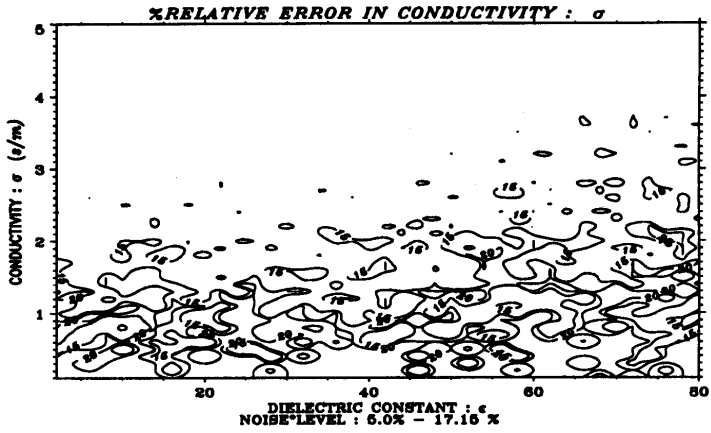

Figure 20. Contour map of percent relative error in conductivities reconstruction for $zero^{th}$ **order:** $a = 0.32652mm, b = 1.0922mm, c = 10.000mm, h = 37.5mm$

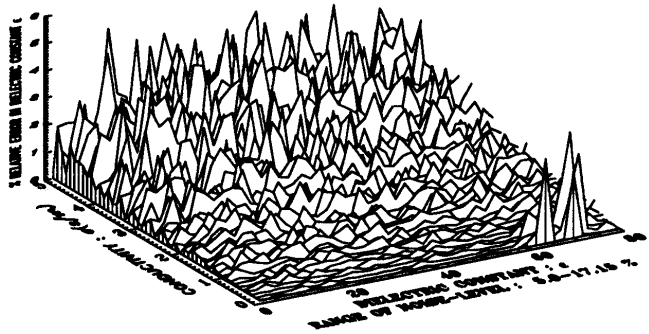

Figure 21. Relief map of percent relative error in dielectric constants reconstruction for $zero^{th}$ order: $a = 0.32652mm, b = 1.0922mm, c = 10.000mm$, $h = 37.5mm$, $(x_{min}\% - x_{max}\%)$

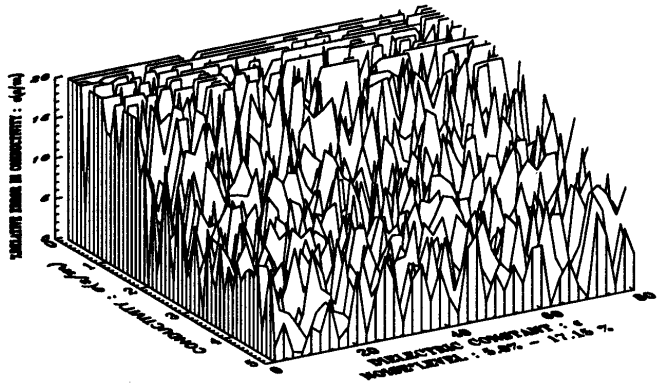

Figure 22. Relief map of percent relative error in conductivities reconstruction for $zero^{th}$ order: $a = 0.32652mm, b = 1.0922mm, c = 10.000mm, h = 37.5mm$, $(x_{min}\% - x_{max}\%)$

4. Conclusion

We have performed herein $Zero^{th}$ order and *MOM* solutions of the integral equation describing our problem. To ensure practical applicability of our model, asymptotic techniques were employed to dramatically accelerate the summations of the infinite series. Plots presented show the edge singularities in the *MOM* solution.

We have derived an expression for the coaxial line reflection coefficient Γ of the *TEM* mode for both $Zero^{th}$ order and *MOM* solutions. It was observed that, even though Γ was defined only for the coaxial *TEM* mode, it had contribution from the higher order modes generated in the aperture. At low losses ($\sigma \to 0$ or high Q), resonance of the shorted waveguide is well defined, but diminishes for higher loss since the excited modes in the cavity are quickly dissipated.

We have solved the inverse problem using *Müller's Method*. An implicit equation was derived for ε_r, the relative complex permittivity of the test samples as a function of Γ and model parameters. Reconstruction of the simulated complex permittivities with *Muller's* algorithm shows exceptional accuracies, except at resonant points. In addition, a noise study of the algorithm was performed using corrupted input data. Overall, the scheme presented has been very successful in modeling the physics of wave propagation in the media and reconstruction of the media from its wave propagation properties. Caution must be exercised to avoid resonant points of the model.

An important limitation of our method is the fact that test samples have to be prepared to fit the geometry of the model. For geophysical logging this may not present any real problem. But in medical applications, where in vivo measurements are a requirement, this becomes a major limitation. Also in nondestructive testing this model is unsuitable. However, the model could be modified in these cases by letting dimensions c and h approach infinity. This will result in an open ended coaxial line into a half-space with perfectly conducting flanges. Stuchly's et al. [1, 3] and Delecki [25] have done extensive work in this area using an equivalent circuit model.

Another limitation of our method is restriction to homogeneous complex permittivity media. For many areas of application, the medium is inherently heterogeneous and must be modeled with variable ε_r.

Acknowledgments.

This paper is an elaboration on the material presented in an invited talk in a special section on Inverse Scattering Methods and Applications at PIERS'95 in Seattle, Washington. The section was organized by T. MḢabashy, C. Torres-Verdin and J. Xia. We thank them for their interest in this work.

References

1. Stuchly, M. A., and S. S. Stuchly, "Coaxial line reflection methods for measuring dielectric properties of biological substances at radio and. microwave frequenciesa review," *IEEE Transactions on Instrumentation and Measurement,* Vol. IM-29, No. 3, 176–183, September 1980.
2. Mosig, J. R., E. Besson Jean-Claude, M. Gex-Fabry, and F. E. Gardiol, "Reflection of an open-ended coaxial lines and application to nondestructive measurement of materials," *IEEE Transactions on Instrumentation and Measurement,* Vol. MI-30, No. 1, 46–51, March 1981.
3. Athey, T. W., M. A. Stuchly, and S. S. Stuchly, "Measurement of radio frequency permittivity of biological tissues with open-ended coaxial line: Part 1," *IEEE Transactions on Microwave Theory and Technique,* Vol. MTT-30, No. 1, 82–86 January 1982.
4. Misra, D. K., "A quasi-static analysis of open-ended coaxial lines," *IEEE Transactions on Microwave Theory and Techniques,* Vol. MTT-35, No. 10, 925–928, October 1987.
5. Staebell, K. F., and D. K. Misra, "Experimental technique for in vivo permittivity measurement of materials at microwave frequencies," *IEEE Transactions on Microwave Theory and Techniques,* Vol. 38, No 3, 337–339, March 1990.
6. Stuchly, S. S., and E. J. Rzepecka, "Permittivity measurements at microwave frequencies using lumped elements," *IEEE Transactions on Instrumentation and Measurement,* Vol. IM-23, No. l, 56–62, March 1974.
7. Baker-Jarvis, J., E. J. Vanzura, and W. A. Kissick, "Improved technique for determining complex permittivity with the transmission/reflection method," *IEEE Transactions on Microwave Theory and Techniques,* Vol. 38, No. 8, 1096–1103, August 1990.

8. Macphie, R. H., M. Opie, and C. R. Ries, "Input impedance of a coaxial line probe feeding a circular waveguide in the TMol mode," *IEEE Transactions on Microwave Theory and Technique,* Vol. 38, No. 3, 334–337, March 1990.
9. Otto, D. V., "The admittance of cylindrical antennas driven from a coaxial line," *Radio Science,* Vol. 2 (New Series), No. 9, 1031–1042, September 1967.
10. Stuchly, M. A., M. M. Brady, S. S. Stuchly, and G. Gajda, "Equivalent circuit of an open-ended coaxial line in lossy dielectric," *IEEE Transactions on Instrumentation and Measurement,* Vol. IM-31, No. 2, 116–119, June 1982.
11 . Stuchly, M. A., M. M. Brady, S. S. Stuchly, and G. Gajda, "Equivalent circuit of an open-ended coaxial line in lossy dielectric," *IEEE Transactions on Instrumentation and Measurement,* Vol. IM-31, No. 2, 116–119, June 1982.
12. Otto, G. P., and W. C. Chew, "Improved calibration of a large open-ended coaxial probe for dielectric measurements," *IEEE Transactions on Instrumentation and Measurement,* Vol. 40, No. 4, 742–746, August 1991.
13. Yan-Zhen, W., and S. Sridhar, "Radiation-corrected open-ended coax line for dielectric measurements of liquids up to 20 GHz," *IEEE Transactions on Microwave Theory and Technique,* Vol. TT-39, No. 3, 526–531, March 1991.
14. Belhadj-Tahar and Fourrier-Lamer, "Broad-band analysis of a coaxial discontinuity used for dielectric measurements," *IEEE Transactions on Microwave Theory and Technique,* Vol. MTT-34, No. 3, 346–350, March 1986.
15. Risley, E. W., JR., "Discontinuity capacitance of a coaxial line terminated in circular waveguide," *IEEE Transactions on Microwave Theory and Techniques,* Vol. MTT-17, No. 2, 86–92, February 1969.
16. Risley, E. W., JR., "Discontinuity capacitance of a coaxial Line terminated in circular waveguide: Part II-Lower bound solution," *IEEE Transactions on Microwave Theory and Techniques,* 564–566, August 1973.
17. Sherman, M. M., "A model for the frequency dependence of the dielectric permittivity of reservoir rocks," *The Log Analyst,* 358–369, September-October 1988.

18. Alvarez, A, "Complex dielectric permittivity in rocks: A method for its measurement and analysis," *Geophysics,* Vol. 38, No. 2, 920–940, October 1973.
19. Nyshadham, A., C. L. Sibbald, and S. S. Stuchly, "Permittivity measurements using open-ended sensor and reference liquid calibr ations an uncertainty analysis," *IEEE Transactions on Microwave Theory and Techniques,* Vol. 40, No. 2, 305–314, February 1992.
20. Dudley, D. G., *Mathematical Foundation for Electromagnetic Theory,* IEEE Press, NJ, Due May 1994.
21. Abramowitz, M., and I. A. Stegun, *Handbook of Mathematical Functions,* Dover Publications, Inc., New York, 1005–1006, 1972.
22. Wright, D. B., D. G. Dudley, and K. F. Casey "Electromagnetic coupling by a wire through a cavity-backed circular aperture in an infinite screen," *IEEE Journal of Electromagnetic waves and Applications,* Vol. 4, No. 5, 375–400, 1990.
23. Muller, D. Z, "A method for solving algebraic equations using an automatic computer, *Mathematical tables and Aids to Computation,* Vol. 10, 208–215, 1956.
24. Collin, R. E., *Field Theory of Guided Waves,* 2nd Edition, IEEE Press, NJ, 811–821, 1991
25. Delecki, Z. A., "Analysis of the open-ended coaxial lines sensors," *IEEE Journal of Electromagnetic waves and Applications,* Vol. 4, No. 2, 169–183, 1990.
26. Taherian, R., D. J. Yuen, T. M. Habashy, and J. A. Kong, "A coaxial-circular waveguide for dielectric measurement," *IEEE Transactions on Geoscience and Remote Sensing,* Vol. 29, No. 2, 321–330, March 1991.